Biophysical Journal

Supporting Material

Pulse Dipolar ESR of Doubly Labeled Mini TAR DNA and Its Annealing to Mini TAR RNA

Yan Sun, Peter P. Borbat, Vladimir M. Grigoryants, William K. Myers, Jack H. Freed, and Charles P. Scholes

SUPPORTING MATERIAL

Table of Contents

Protocol for Anion Exchange HPLC Purification of Spin-Labeled mini TAR DNA.

Anion-exchange HPLC was used to remove the excess nitroxide spin label from the reaction mixture and to separate unlabeled and partially labeled mini TAR DNA from doubly-labeled. The reaction mixture was subjected to anion-exchange HPLC using a PA-100 column (4 X 250 mm^2, Dionex Inc., Sunnyville, CA) at a pressure of approximately 2000 psi. (For later work a Biorad FPLC unit, which would produce 1200 psi, was employed.) Nucleic acids were eluted using a low salt stationary phase (buffer A: 1 mM $NaClO_4$, 20mM Tris–HCl, pH 6.8 and 20% v/v acetonitrile) and a high salt mobile phase (buffer B: 400 mM $NaClO_4$, 20 mM Tris–HCl, pH 6.8, and 20% v/v acetonitrile). Oligonucleotides were detected via absorbance at 260 nm. The data shown in **Figure S1** were obtained using the PA-100 column with a flow rate of 2 mL min^{-1} with the linear gradient shown in the adjacent table. The doubly-labeled mini TAR DNA elutes more rapidly than the unlabeled TAR DNA due to the loss of negative charge upon spin probe attachment. The fractions were concentrated and buffer exchanged with water using the Amicon Ultra-3k MWCO centrifugation filter. Desalted samples were lyophilized and stored at -80 °C.

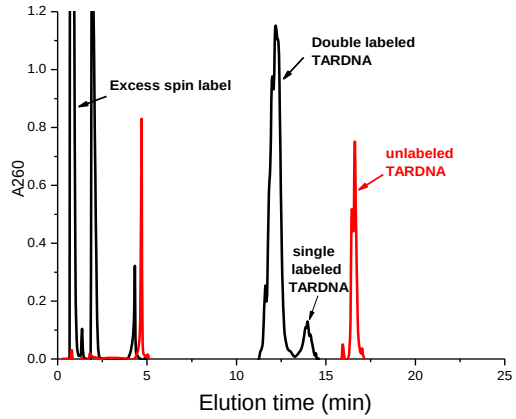

Step	Elution(min)		%Bufr B	
	start	End	Start	End
1	0	1.8	0	0
2	1.8	3.8	0	15
3	3.8	18.8	15	30
4	18.8	19.8	30	100
5	19.8	24.8	100	100
6	24.8	29.8	0	0

Fig. S1. Anion-exchange HPLC traces. The black trace is the 260-nm absorbance of a crude TAR DNA strand with two labeled phosphorothioate groups, and the red trace is the corresponding TAR DNA before labeling. The sample was doubly-labeled SLAB. The table provides the linear gradient profile.

Protocol for mini TAR DNA Analysis by Denaturing PAGE.

A nucleic acid sequencer from CBM Scientific was employed for analytical denaturing polyacrylamide gel electrophoresis (PAGE) to separate labeled and unlabeled mini TAR DNA and to monitor the extent of the reactions shown in **Fig. 2** in the main text. Analytical gels (20 cm) were made according to the manufacturer's specifications from a 25 mL solution of 20 % polyacrylamide (acrylamide: bis = 19:1) with 7 M urea in 1 X TBE (Tris-borate-EDTA) buffer, 250 μL of 10% APS (ammonium persulfate), 25 μL of N,N,N', N'-Tetramethylethylenediamine (TEMED). The running buffer was 1 X TBE. Gels were run at room temperature at 15 W and 500 V for about 2 hours. The separation of unlabeled, singly-labeled, and doubly-labeled mini TAR DNA is shown in **Figure S2**. Denaturing P. can be used on a preparative scale for separation of labeled and unlabeled mini TAR; however, the process can lead to loss of spin paramagnetism, possibly by reduction, and HPLC purification was preferred (1).

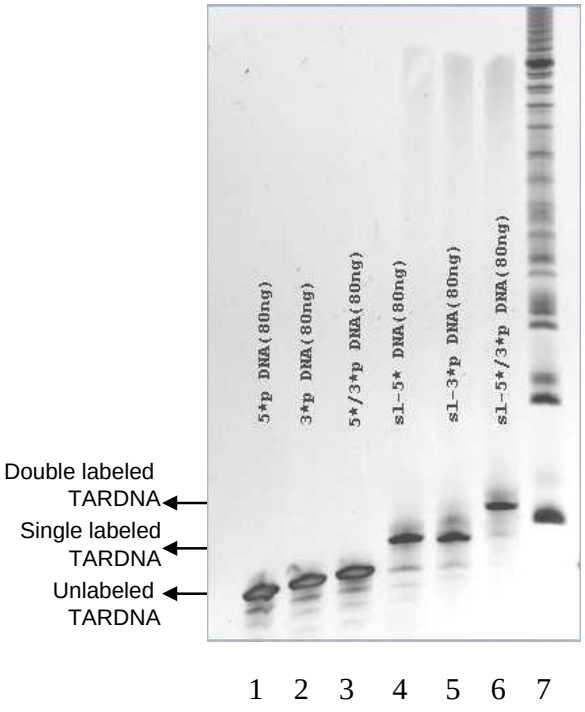

Fig. S2. This figure provides gel results showing the SLA, SLB, SLAB bands before and after spin label reaction. Lane 1: mini TAR DNA with phosphorothioate at SLA (3.0 pmoles); Lane 2: mini TAR DNA phosphorothioate at SLB (3.0 pmoles); Lane 3: mini TAR DNA phosphorothioates at SLAB (3.0 pmoles each); Lane 4: SLA after reaction; Lane 5: SLB after reaction; Lane 6: SLAB after reaction, (3.0 pmoles); Lane 7: 10 bp DNA ladder, from which the lowest band shown is from denatured 30 bp DNA.

Gel Shift Annealing Assay.

The annealing of mini TAR DNA with complementary mini TAR RNA in the presence of increasing amounts of NCp7 is the functional assay to compare the relative annealing effectiveness of doubly-labeled mini TAR DNA and unlabeled mini TAR DNA (2, 3). The gel was a 20 % polyacrylamide gel. Mixtures of mini TAR DNA, mini TAR RNA, and NCp7 were allowed to equilibrate for five minutes at room temperature in 20 mM HEPES buffer, 20 mM Na^+, 0.2 mM Mg^{2+}, pH 7.5. Gels were run at 4 ºC for 1.5 hours at 120 V. Experiments were performed at constant mini TAR DNA and mini TAR RNA concentrations of 1.4 μM. In separate lanes the TAR DNA: TAR RNA: NCp7 ratios were changed from 1:0:0 to 1:1:0 to 1:1:1 to 1:1:4.

Figures S3 a,b,c respectively contained unlabeled mini TAR DNA, doubly-labeled SLAB mini TAR DNA, and SLCD doubly-labeled mini TAR DNA. In these figures the first lane, which is mini TAR DNA stands alone and travels fastest. The second lane shows a 1:1 ratio of TAR DNA to TAR RNA, and in this lane there is evidence for the mini TAR DNA by itself, for a mini TAR RNA by itself with its band traveling slower, and for a small amount of annealed duplex, which travels slower than either of the two former bands. As respectively shown in the third and fourth lanes, the ratio of NCp7: TAR RNA: TAR DNA was then changed from 1:1:1 to 1:1:4. With increasing NCp7, the amount of annealed duplex increased for all TAR DNA constructs, both labeled and unlabeled. Compared to the lanes with unlabeled mini TAR DNA, the doubly-labeled forms of TAR DNA, showed similar annealing patterns to the unlabeled and to each other as they annealed in the presence of NCP7. The implication is that doubly-labeled constructs do not perturb the annealing function of NCp7 as it converted complementary hairpin TAR DNA and hairpin TAR RNA to a duplex.

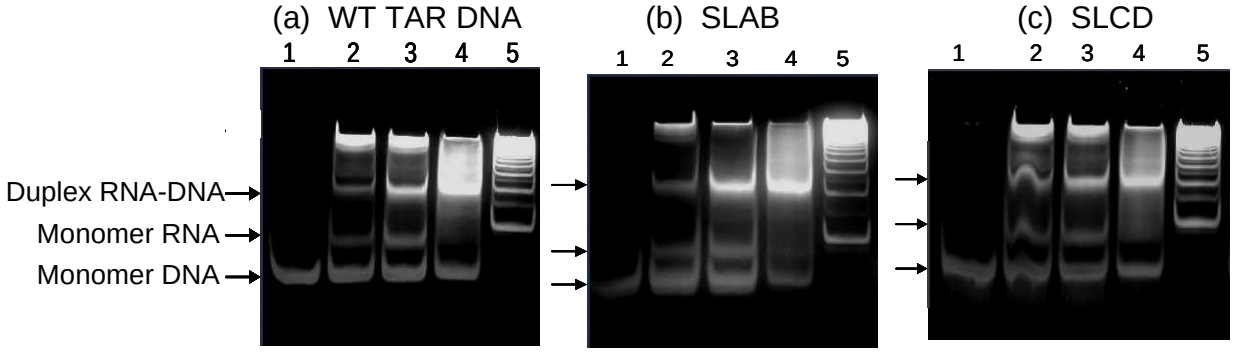

Fig. S3. This figure presents the annealing of mini TAR RNA with mini TAR DNA or with the doubly-labeled derivatives of mini TAR DNA in the presence of increasing amounts of NCp7. Non-denaturing buffer conditions were: 20 mM HEPES buffer, 20 mM Na^+, 0.2 mM Mg^{2+}, pH 7.5. Traces (**a**), (**b**), and (**c**) respectively used: (**a**) unlabeled WT mini TAR DNA; (**b**) doubly-labeled SLAB; (**c**) doubly labeled SLCD. The conditions for lanes were as follows: Lane 1, free TAR DNA; Line 2, TAR DNA: TAR RNA, 1:1 with no NCp7; Lane 3, TAR DNA: TAR RNA: NCp7, 1:1:1; Lane 4, TAR DNA: TAR RNA: NCp7, 1:1:4; Lane 5: 10 bp DNA ladder.

DEER Dipolar Evolution Transients.

Figs. S4, S5, and **S6** below provide the 17.6 GHz DEER time evolution data that were used to reconstruct the respective distance distributions in **Figs. 4, 5,** and **6** in the main text. The data in the figures below are plotted background-corrected as described in the Methods and Materials section of the main text. All data were normalized to represent the DEER signal, which is unity at zero time, and distributed vertically for clarity.

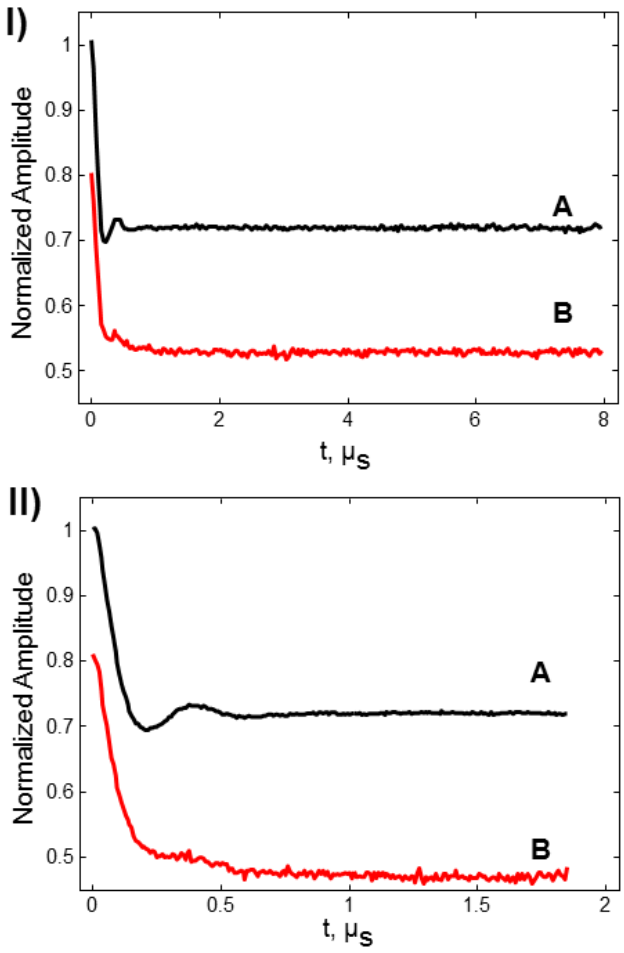

Fig. S4. These are the time evolution data corresponding to the DEER distributions in **Fig. 4A and 4B** in the Results Section. Here, the transients labeled **A** are for SLCD by itself and correspond to the DEER distribution of **Fig. 4A**. The transients labeled **B** are for SLCD with the addition of 4 equivalents of NCP7 and correspond to the DEER distribution of **Fig. 4B**. The transients are shown over both a longer time view (Panel I) of ~8 μs, which provided information on the presence of inter-label distances greater than 60 Å, and over a shorter time view (Panel II) of ~2 μs, which was used to reconstruct the inter-label distribution below 60 Å. Distance distributions were generated from short-term data; long term data served to verify the absence of very long distances. Data averaging times for Panel (**I**) were 54 min (A), 15 h (B) and for Panel (**II**) both (A) and (B) were 30 min. All data were taken at 65 ºK.

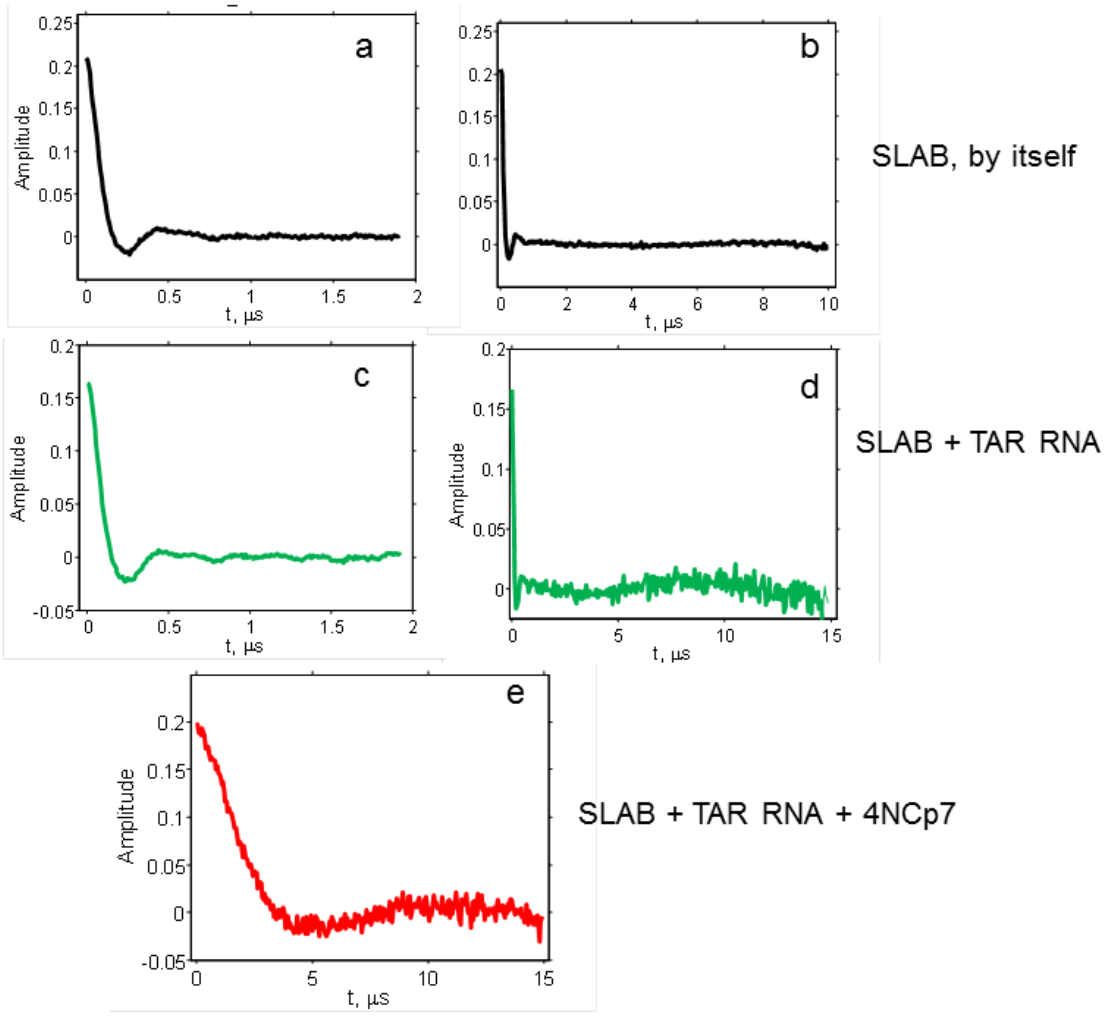

Fig. S5. These are the time evolution data corresponding to the DEER distributions in **Fig. 5** in the Results Section for: SLAB DNA by itself, SLAB DNA+ TAR RNA with no NCp7, and SLAB DNA + TAR RNA + 4X NCp7. The time domain data recorded over approximately 2 µs were sufficient to reconstruct the inter-label distributions, P(r), below 60 Å for SLAB DNA by itself and SLAB DNA+ TAR RNA with no NCp7. The time-domain data of the dipolar evolution, recorded over 15 µs, were sufficient to reconstruct the distance of ~7.5 nm for the duplex RNA-DNA arising from SLAB DNA + TAR RNA + 4X NCp7. Deuterated solutions and low ionic strength were used in all three cases. Data averaging time were as follows: Panel (**a)**, 30 min; Panel (**b)**, 3 h; Panel (**c)**, 30 min; Panel (**d)**, 14 hr; Panel (**e)**, 11.5 hr. All data were taken at 65 ºK.

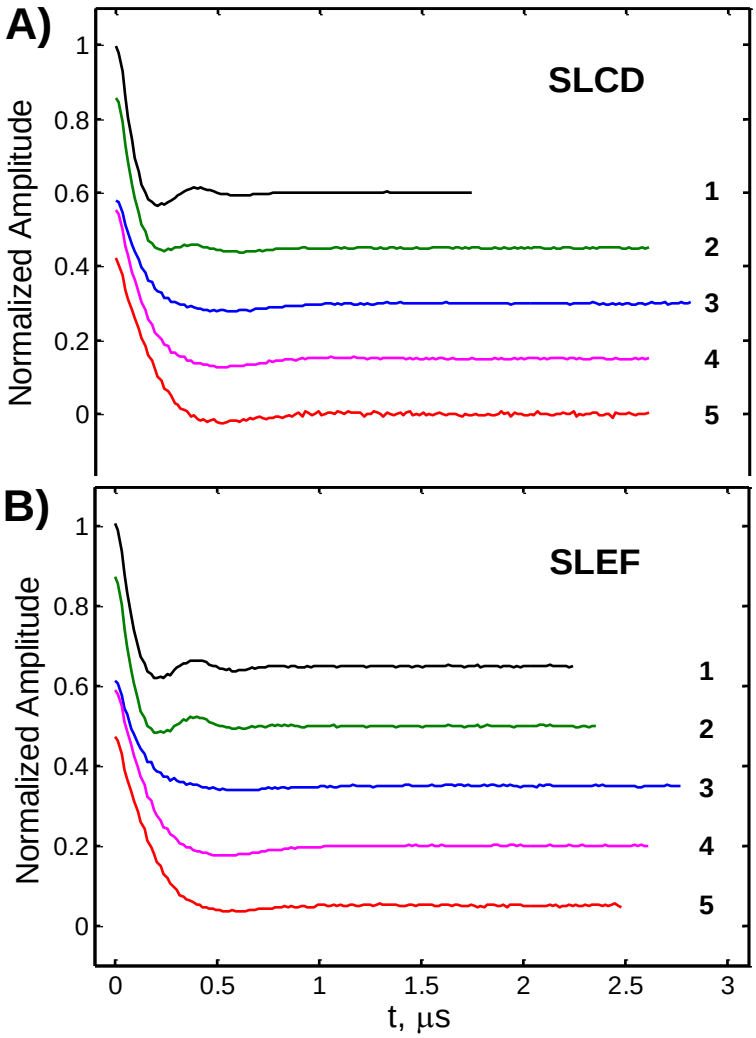

Fig. S6. These are the time evolution data corresponding to the DEER distributions, P(r), shown in **Figs. 6 a** and **6 b** of the main text and in **Figs. S8** and **S9**. The data in the figure are plotted background-corrected as described in the Materials and Methods section of the main text. Panel (A) corresponds to SLCD. Here, individual curves use color-coding of the respective panels in the main text and additionally are numbered as: (1) black, SLCD by itself; (2) green, a 1:1 mixture of SLCD + mini TAR RNA; (3) blue, a thermally-annealed mixture of 1:1 mixture of doubly-labeled SLCD and mini TAR RNA; (4) magenta, a 1:1:1 mixture of SLCD mini TAR DNA to mini TAR RNA to NCp7; (5) red, a 1:1:4 mixture of SLCD mini TAR DNA to mini TAR RNA to NCp7. Panel (B) is for SLEF and has the same time-scale, color-coding, and data numbering as Panel (**A**). Data averaging time for SLCD was 10 min for data set (1) and 43 min for the rest. For SLEF these were 10 min for (1), 21 min for (2) and (5), and 43 min for (3) and (4). All data were taken at 65 K.

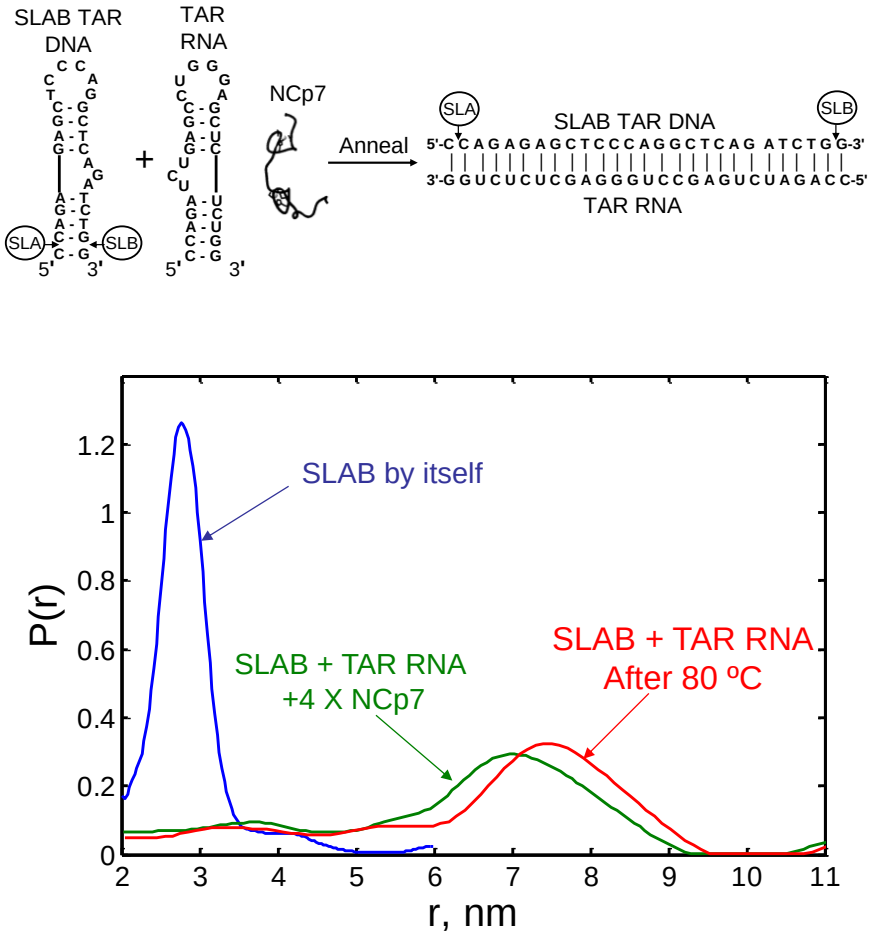

Fig. S7. A comparison of the inter label distance distribution taken in protonated solvent between doubly-labeled SLAB mini TAR DNA by itself (blue trace), doubly-labeled SLAB mini TAR DNA annealed in the presence of a 1:1:4 of SLAB mini TAR DNA to unlabeled mini TAR RNA: to NCp7 (green trace) , and doubly-labeled SLAB mini TAR DNA thermally annealed at 80 ºC with mini TAR RNA (red trace). Sample conditions: 20 mM HEPES, 20 mM NaCl, 0.2 mM $MgCl_2$, pH 7.5. Samples were frozen in 10 % glycerol to prevent tube breakage. These were early samples prepared in protonated solvent, and the position of the peaks at long distances (> 60 Å) is only accurate to within 5 Å. The purpose of the figure is to show the similarity of the NCp7-annealed and the thermally annealed 1:1 mixtures of TAR DNA and TAR RNA.

Calculated Inter-NO Distances – Comparison of DEER Experimental Results and NASNOX Predictions

Using NASNOX, an average inter-label NO distance $\langle r_{NASNOX} \rangle$ was calculated from the ensemble of allowed rotamers, and the RMS uncertainty σ_{NASNOX} in the distance between NO groups determined. For a Gaussian distribution of inter-nitroxide distances, this latter uncertainty σ translates readily into the full-width at half height, $W_{1/2}$, of the double-label distance distribution, where $W_{1/2} = (2)^{3/2} (0.693)^{1/2} \sigma$. Predicted distances and widths of the inter-nitroxide distance distribution were then compared to corresponding experimental DEER results $\langle r_{DEER} \rangle$ and σ_{DEER}. Additionally, histograms of the double-label inter-nitroxide distance distribution were computed from NASNOX ensembles (4, 5) for comparison to the experimentally determined distributions obtained by PDS. An overlay of PDS results for SLCD (**Fig. 6a**) and SLEF (**Fig. 6b**) and the corresponding histograms of the expected distance distributions for the double labels are provided in the **Supporting Material, Figs. S8** and **S9**. The histograms shown in **Figs. S8** and **S9** were obtained both for the double labels residing in the unperturbed mini TAR DNA upper stem-loop and for the double labels of SLCD and SLEF residing in the DNA-RNA duplexes.

In **Table S1** the experimentally measured distances between diametrically opposite nitroxide doubly-labeled sites in SLAB, SLCD, and SLEF doubly-labeled forms of mini TAR DNA were all found within 1 Å of $\langle r_{DEER} \rangle$ = 27 Å with inter-nitroxide distribution widths which diminished in the order SLAB, SLCD, SLEF. Using a dodecamer B-form DNA duplex (PDB 1CS2 (6, 7)) and NASNOX, the NO groups of eleven separate, diametrically opposite spin labels provided estimates of $\langle r_{NASNOX} \rangle$ = 26.0 Å and σ_{NASNOX} = 1.9 Å, both in good agreement with our experiments on diametrically opposite labels in duplex regions of mini TAR DNA. Since the inter-phosphorous distance between diametrically opposed phosphates is 17.7 Å (7) and the average inter-nitroxide distance of diametrically opposite nitroxides per **Table S1** was 26.9 Å, then the additional radial distance of a spin label NO group from its attaching phosphorothioate would be about 4.6 Å [= (26.9 – 17.7)/2].

Using a 13-mer DNA-RNA duplex model (PDB 1EFS (8), application of NASNOX with spin labels attached *in silico* provided from DNA-RNA duplexes estimates of the expected values of $\langle r_{NASNOX} \rangle$ and σ_{NASNOX}. Between spin labels attached 10 bases apart in the DNA strand of the RNA-DNA duplex it was found that $\langle r_{NASNOX} \rangle$ = 36.5 Å and σ_{NASNOX} = 4.7 Å (8), to be compared with $\langle r_{DEER} \rangle$ = 34.8 Å and σ_{DEER} = 5.9 Å from SLEF in the mini TAR DNA-RNA complex. Between spin labels attached 8 bases apart to the DNA strand of the RNA-DNA duplex it was found that $\langle r_{NASNOX} \rangle$ = 36.3 Å and σ_{NASNOX} = 4.6 Å, to be compared with $\langle r_{DEER} \rangle$ = 35.1 Å and σ_{DEER} = 4.6 Å from SLCD in the mini TAR DNA-RNA complex. In both cases the agreement between experiment and prediction was good. The similarity of inter-NO distances of SLCD, 8 bases apart, and SLEF, 10 bases apart, follows because the distance change along the direction of the helix is offset by the distance change due to helical rotation of nitroxide side chains perpendicular to the helical axis.

To approximate the distance on the mini TAR DNA strand between phosphorothioate-attached spin labels near the opposite ends of the 27-mer duplex as SLA and SLB would be after they are incorporated in a TAR DNA-RNA duplex, we have estimated distances from the axial rise per residue and the angular rotation per residue about the helix axis (9, 10). The rise based on the

average of four different RNA-DNA duplexes, is 2.90 ± 0.08 Å/base, and the rotation per residue is 32 ± 1º (9). Per our own work on diametrically opposite bi-labels, the distance of the label nitroxide from the helix axis is 13.5 Å. For a 25 phosphate separation, these numbers (rise per base, rotation per residue, and distance of nitroxide from helix axis) predict a distance between labels of $\langle r \rangle$ = 74.5 ± 2.8 Å. This simple geometric approach assumes a straight helix. The literature indicates that there can be some local mixture and flexibility variation between A-type and B-type helical forms within the mixed RNA-DNA helix (9); such mixture and flexibility may contribute to the 19.5 Å breadth of the SLA-SLB distance distribution in the RNA-DNA duplex. Given the approximate way of estimating the long SLA-SLB inter-nitroxide distance, the agreement between prediction and DEER results is good.

Table S1.
Inter-label Distances and Peak Widths of Doubly-Labeled mini TAR DNA

Experimental DEER Inter-label Distances and Widths				**Computed Estimates, Inter-label Distances and Widths**
Sample	**$\langle r_{DEER} \rangle$ (Å)**[a]	**$W_{1/2}$ (Å)**[a]	**σ_{DEER} (Å)**[a]	
SLAB by itself	27.5 ± 0.5	7.0 ± 0.5	3.0 ± 0.2	$\langle r_{NASNOX} \rangle$ = 26.0 Å σ_{NASNOX} = 1.9 Å (b)
SLCD by itself	26.8 ± 0.4	5.2 ± 0.4	2.2 ± 0.2	
SLEF by itself	26.3 ± 0.4	4.3 ± 0.4	1.8 ± 0.2	
1:1:4 SLCD/mini TAR RNA/NCp7	35.1 ± 0.6	10.8 ± 1.0	4.6 ± 0.4	$\langle r_{NASNOX} \rangle$ = 36.3 Å σ_{NASNOX} = 4.6 Å (c)
1:1:4 SLEF/mini TAR RNA/NCp7	34.8 ± 0.6	14.0 ± 1.0	5.9 ± 0.4	$\langle r_{NASNOX} \rangle$ = 36.5 Å σ_{NASNOX} = 4.7 Å (d)
1:1:4 SLAB/mini TAR RNA/NCp7	76.5 ± 2.0	19.5 ± 2.0	8.3 ± 0.8	$\langle r \rangle$ = 74.5 ± 2.8 Å (e)

[a] $\langle r_{DEER} \rangle$ and $W_{1/2}$ are the respective experimental inter-label distance and the full peak width at half height as determined experimentally by DEER. σ_{DEER} is the RMSD of the DEER peak, and assuming a Gaussian shape, $W_{1/2} = (2)^{3/2} (0.693)^{1/2} \sigma_{DEER}$.

[b] By use of the dodecamer DNA duplex (PDB 1CS2) (6, 7) and NASNOX algorithm, the NO groups of eleven separate, diametrically opposite spin labels provided this estimate of $\langle r_{NASNOX} \rangle$ and σ_{NASNOX} .

[c] By use of a 13-mer DNA-RNA duplex (PDB 1EFS) (8) and the NASNOX algorithm, doubly-labeled DNA sites 8 bases apart, like SLC and SLD, were predicted to have these values for $\langle r_{NASNOX} \rangle$ and σ_{NASNOX} .

[d] By use of a 13-mer DNA-RNA duplex (PDB 1EFS) (8) and the NASNOX method, double-labeled DNA sites 10 bases apart, like SLE and SLF, were predicted to have these values for $\langle r_{NASNOX} \rangle$ and σ_{NASNOX} .

[e] Based on an axial rise of 2.90 ± 0.08 Å/base, a helical rotation per residue of 32 ± 1º (9) a separation between labeling sites of 25 phosphates, and a radial distance of the label nitroxide from the helix axis of 13.5 Å (per **Table S1** above) , this distance $\langle r \rangle$ was geometrically predicted.

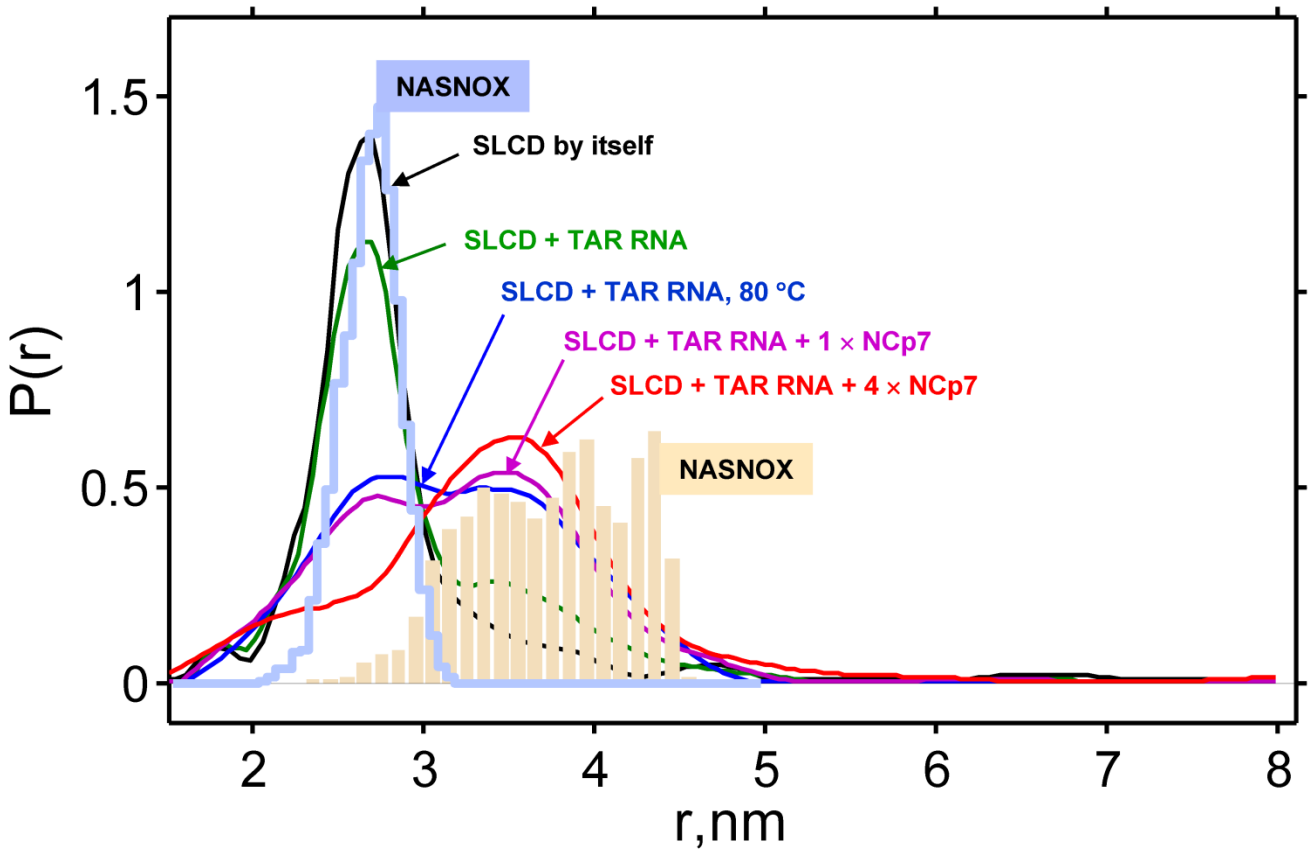

Fig. S8. The inter-nitroxide distance distribution from SLCD shown in **Fig. 6a** in the main text compared to the histograms of the distance distributions computed by NASNOX for the following: 1) The histogram (light blue) for a diametrically opposite pair of phosphorothioate-attached spin labels located on a duplex DNA strand specifically from PDB structure 1CS2, bases 6 & 20 from ref. (6)). 2) The histogram (beige) for a pair of phosphorothioate-attached spin labels 8 bases apart on the DNA strand of a DNA-RNA duplex (specifically from the PDB structure 1EFS, bases 3 & 11 from ref. (8).

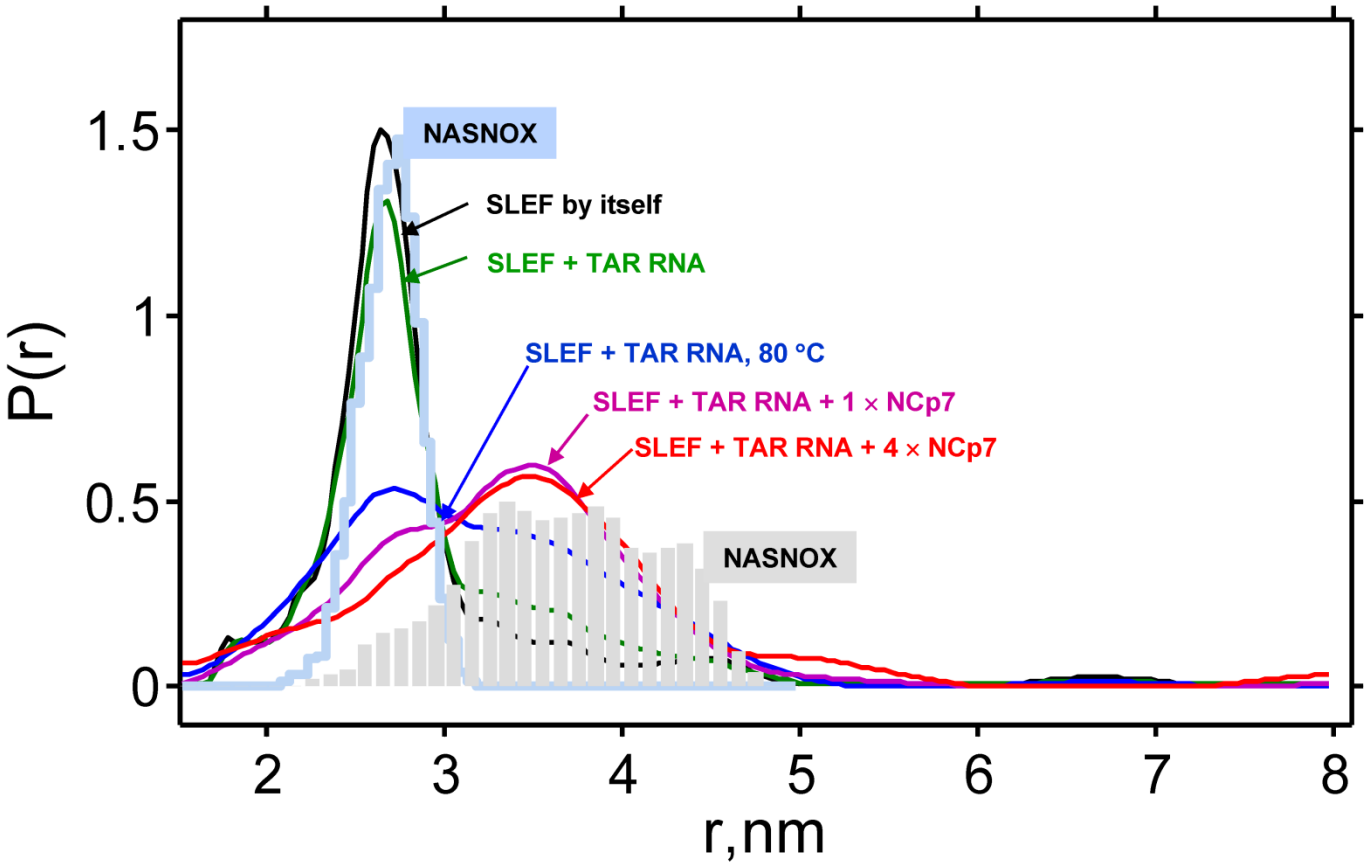

Fig. S9. A comparison of the inter-nitroxide distance distribution from SLEF shown in **Fig. 6b** in the main text to the histograms of the distance distributions computed by NASNOX for the following: 1) The histogram (light blue) for a diametrically opposite pair of phosphorothioate-attached spin labels located on a duplex DNA strand (specifically from PDB structure 1CS2, bases 6 & 20 from ref. (6)). 2) The histogram (grey) for a pair of phosphorothioate-attached spin labels 10 bases apart on the DNA strand of a DNA-RNA duplex (specifically from the PDB structure 1EFS, bases 2 & 12 from ref. (8).

PDS Versus Fluorescence Resonance Energy Transfer (FRET) in Application to TAR.

The technique of FRET at different levels of sophistication has been used to follow inter-probe distance change, conformational bending, and annealing of TAR DNA and TAR RNA in the presence of NCp7 (11-18). Solution FRET initially provided qualitative information about RNA unwinding and annealing in the presence of NCp7 (12, 13). Time-resolved FRET decay has provided evidence for different species with several different decay times, and by inference, evidence for several different conformations of frayed, destabilized TAR DNA (19, 20). FRET correlation spectroscopy showed evidence for the kinetic interconversion of destabilized stem loops (21, 22). More elegant single molecule FRET, requiring resolution of individual, immobilized, fluorescently labeled biomolecules has provided histograms of single molecule FRET efficiencies. The evidence from these histograms, which were taken under ambient temperature conditions, is that interconverting conformers of duplex and stem-loop structures were brought about by NCp7 (11, 14-18). Such distributions may well translate into conformers with different inter-label distances, but it is noteworthy that FRET histograms are appropriately shown as a function of FRET efficiency not of inter-probe distance (11). The Förster mechanism for FRET has in principle an r^{-6} inter-fluorophore distance dependence but with somewhat uncertain factors as discussed by Gopich and Szabo (23). Also, FRET requires a larger probe size and longer tethers than nitroxide probes, as well as the need of multiple FRET pairs of different Förster radii to cover a distance range of, e.g., 1-10 nm. The probe orientation factor for FRET often needs to be determined independently. The r^{-3} inter-nitroxide distance dependence of PDS means that PDS will more directly yield structural information over the 1-9 nm range, including distance distributions and multiple conformers. The aggregating properties of 1-55 NCp7, which are essential to its annealing behavior, are an impediment to the fluorescence process because of the light scattering of aggregates. In brief, PDS and FRET complement each other for study of oligonucleotide structures; PDS gives more detailed distance information, and FRET is at present more amenable to ambient temperature measurements.

REFERENCES

1. Sun, Y., Z. Zhang, V. M. Grigoryants, W. K. Myers, F. Liu, K. A. Earle, J. H. Freed, and C. P. Scholes. 2012. The Internal Dynamics of Mini c TAR DNA Probed by Electron Paramagnetic Resonance of Nitroxide Spin-Labels at the Lower Stem, the Loop, and the Bulge. Biochemistry 51:8530–8541.
2. Vo, M. N., G. Barany, I. Rouzina, and K. Musier-Forsyth. 2006. Mechanistic studies of mini-TAR RNA/DNA annealing in the absence and presence of HIV-1 nucleocapsid protein. J Mol Biol 363:244-261.
3. Vo, M. N., G. Barany, I. Rouzina, and K. Musier-Forsyth. 2009. HIV-1 nucleocapsid protein switches the pathway of transactivation response element RNA/DNA annealing from loop-loop "kissing" to "zipper". J Mol Biol 386:789-801.
4. Price, E. A., B. T. Sutch, Q. Cai, P. Z. Qin, and I. S. Haworth. 2007. Computation of nitroxide-nitroxide distances in spin-labeled DNA duplexes. Biopolymers 87:40-50.
5. Qin, P. Z., I. S. Haworth, Q. Cai, A. K. Kusnetzow, G. P. Grant, E. A. Price, G. Z. Sowa, A. Popova, B. Herreros, and H. He. 2007. Measuring nanometer distances in nucleic acids using a sequence-independent nitroxide probe. Nat Protoc 2:2354-2365.
6. Leporc, S., O. Mauffret, G. Tevanian, E. Lescot, M. Monnot, and S. Fermandjian. 1999. An NMR and molecular modelling analysis of d(CTACTGCTTTAG). d(CTAAAGCAGTAG) reveals that the particular behaviour of TpA steps is related to edge-to-edge contacts of their base-pairs in the major groove. Nucleic Acids Res 27:4759-4767.
7. Cai, Q., A. K. Kusnetzow, W. L. Hubbell, I. S. Haworth, G. P. Gacho, N. Van Eps, K. Hideg, E. J. Chambers, and P. Z. Qin. 2006. Site-directed spin labeling measurements of nanometer distances in nucleic acids using a sequence-independent nitroxide probe. Nucleic Acids Res 34:4722-4730.
8. Hantz, E., V. Larue, P. Ladam, L. Le Moyec, C. Gouyette, and T. Huynh Dinh. 2001. Solution conformation of an RNA--DNA hybrid duplex containing a pyrimidine RNA strand and a purine DNA strand. Int J Biol Macromol 28:273-284.
9. Gyi, J. I., A. N. Lane, G. L. Conn, and T. Brown. 1998. Solution structures of DNA.RNA hybrids with purine-rich and pyrimidine-rich strands: comparison with the homologous DNA and RNA duplexes. Biochemistry 37:73-80.
10. Saenger, W. 1984. Principles of Nucleic Acid Structure. Springer-Verlag, New York.
11. Wang, H., K. Musier-Forsyth, C. Falk, and P. F. Barbara. 2013. Single-molecule spectroscopic study of dynamic nanoscale DNA bending behavior of HIV-1 nucleocapsid protein. The journal of physical chemistry. B 117:4183-4196.
12. Chan, B., K. Weidemaier, W. T. Yip, P. F. Barbara, and K. Musier-Forsyth. 1999. Intra-tRNA distance measurements for nucleocapsid proteindependent tRNA unwinding during priming of HIV reverse transcription. Proc Natl Acad Sci U S A 96:459-464.
13. Hong, M. K., E. J. Harbron, D. B. O'Connor, J. Guo, P. F. Barbara, J. G. Levin, and K. Musier-Forsyth. 2003. Nucleic acid conformational changes essential for HIV-1 nucleocapsid protein-mediated inhibition of self-priming in minus-strand transfer. J Mol Biol 325:1-10.
14. Cosa, G., E. J. Harbron, Y. Zeng, H. W. Liu, D. B. O'Connor, C. Eta-Hosokawa, K. Musier-Forsyth, and P. F. Barbara. 2004. Secondary structure and secondary structure dynamics of DNA hairpins complexed with HIV-1 NC protein. Biophys J 87:2759-2767.

15. Liu, H. W., G. Cosa, C. F. Landes, Y. Zeng, B. J. Kovaleski, D. G. Mullen, G. Barany, K. Musier-Forsyth, and P. F. Barbara. 2005. Single-molecule FRET studies of important intermediates in the nucleocapsid-protein-chaperoned minus-strand transfer step in HIV-1 reverse transcription. Biophys J 89:3470-3479.
16. Liu, H. W., Y. Zeng, C. F. Landes, Y. J. Kim, Y. Zhu, X. Ma, M. N. Vo, K. Musier-Forsyth, and P. F. Barbara. 2007. Insights on the role of nucleic acid/protein interactions in chaperoned nucleic acid rearrangements of HIV-1 reverse transcription. Proc Natl Acad Sci U S A 104:5261-5267.
17. Zeng, Y., H. W. Liu, C. F. Landes, Y. J. Kim, X. Ma, Y. Zhu, K. Musier-Forsyth, and P. F. Barbara. 2007. Probing nucleation, reverse annealing, and chaperone function along the reaction path of HIV-1 single-strand transfer. Proc Natl Acad Sci U S A 104:12651-12656.
18. Wang, H., Y. S. Yeh, and P. F. Barbara. 2009. HIV-1 nucleocapsid protein bends double-stranded nucleic acids. J Am Chem Soc 131:15534-15543.
19. Beltz, H., E. Piemont, E. Schaub, D. Ficheux, B. Roques, J. L. Darlix, and Y. Mély. 2004. Role of the structure of the top half of HIV-1 cTAR DNA on the nucleic acid destabilizing activity of the nucleocapsid protein NCp7. J Mol Biol 338:711-723.
20. Bernacchi, S., S. Stoylov, E. Piemont, D. Ficheux, B. P. Roques, J. L. Darlix, and Y. Mély. 2002. HIV-1 nucleocapsid protein activates transient melting of least stable parts of the secondary structure of TAR and its complementary sequence. J Mol Biol 317:385-399.
21. Beltz, H., J. Azoulay, S. Bernacchi, J. P. Clamme, D. Ficheux, B. Roques, J. L. Darlix, and Y. Mély. 2003. Impact of the terminal bulges of HIV-1 cTAR DNA on its stability and the destabilizing activity of the nucleocapsid protein NCp7. J Mol Biol 328:95-108.
22. Godet, J., and Y. Mély. 2010. Biophysical studies of the nucleic acid chaperone properties of the HIV-1 nucleocapsid protein. RNA Biol 7:687-699.
23. Gopich, I. V., and A. Szabo. 2011. Theory of Single-Molecule FRET Efficiency Histograms. In Single-Molecule Biophysics. John Wiley & Sons, Inc. 245-297.